Reliability assessment of stability of underground rock caverns

Goh, Anthony Teck Chee; Zhang, Wengang

2012

Goh, A. T. C., & Zhang W. (2012). Reliability assessment of stability of underground rock caverns. International Journal of Rock Mechanics and Mining Sciences, 55, 157-163.

https://hdl.handle.net/10356/79469

https://doi.org/10.1016/j.ijrmms.2012.07.012

Reliability Assessment of Stability of Underground Rock Caverns

A.T.C. Goh, W.G. Zhang

School of Civil & Environmental Engineering, Nanyang Technological University

Block N1, Nanyang Avenue, Singapore 639798, Singapore

Corresponding author. Tel.:+65 6790-5271

E-mail address: ctcgoh@ntu.edu.sg

Abstract

Conventional stability assessment of underground tunnels and caverns involves the determination of a factor of safety in which failure is assumed to occur when the load (stress) of the system exceeds the resistance. It is widely recognized that a deterministic analysis of the factor of safety gives only a partial representation of the true margin of safety, since the uncertainties in the design parameters affect the probability of failure. In this paper, a simplified procedure is proposed for evaluating the probability of stress-induced instability for deep underground rock caverns for preliminary design applications. Extensive parametric studies were carried out using the finite difference program FLAC^{3D} to determine the factor of safety for caverns of various dimensions and rock mass strength. Subsequently, the limit state surface was determined through an artificial neural network approach following which a simplified reliability method of evaluating the probability of failure was developed.

Keywords: neural networks; probability of failure; reliability index; rock cavern; safety factor; stability.

1. Introduction

One of the major considerations in the design of an underground rock cavern is the evaluation of its stability since the excavation of the rock causes a redistribution of the stresses in the proximity of the underground opening. Various methods have been proposed to assess the cavern stability, and to assess the necessary support system to maintain the stability of the excavation. Common empirical methods include the use of rock classification systems such as the rock mass rating *RMR* [1] and *Q* methods [2]. Common numerical methods used to evaluate cavern stability can be categorized as continuum methods such as the Finite Element Method (FEM) [3] and Finite Difference Method (FDM) [4], and discontinuum methods such as the Distinct Element Method (DEM) [5] and the Discontinuous Deformation Analysis (DDA) [6]. The selection of a continuum or discontinuum approach depends on the size or scale of the discontinuities with respect to the size or scale of the problem that needs to be solved. There are no universal quantitative guidelines to determine when one method should be used instead of the other [7].

Conventional deterministic evaluation of stability of geotechnical structures and underground openings involves the use of a factor of safety *FS* which considers the relationship between the resistance *R* and the load (stress) *S*. The boundary separating the safe and failure domain is the limit state surface (boundary) defined as:

$$G(\mathbf{x}) = R - S = 0 \tag{1}$$

where $\boldsymbol{x}$ denotes the vector of the random variables. Mathematically, $R > S$ or $G(\boldsymbol{x}) > 0$ would denote a 'safe' domain, and $R < S$ or $G(\boldsymbol{x}) < 0$ would denote a 'failure' domain. For underground caverns, the limit state surface $G(\boldsymbol{x})$ is not known explicitly. Instead, it may be known only implicitly through a numerical procedure such as the finite element method. Therefore, the failure domain only can be found through repeated point-by-point numerical analyses with different input values. A closed-form limit state surface then is constructed artificially using polynomial regression methods.

However, polynomial regression models become computationally impractical for problems involving a large number of random variables and nonlinear limit state functions, particularly when mixed or statistically dependent random variables are involved. An alternative modeling

technique is the use of neural networks. A neural network is a computer model whose architecture essentially mimics the knowledge acquisition and organizational skills of the human brain. A neural network consists of a number of interconnected neurons, which are logically arranged into two or more layers and interact with each other via weighted connections. These weights determine the nature and strength of the influence between the interconnected neurons. There is an input layer where data are presented to the neural network, and an output layer that holds the response of the network to the input. It is the intermediate layers, also known as hidden layers that enable these networks to represent and compute complicated associations between patterns. The back-propagation neural network (BPNN) learning algorithm is widely used because of the simplicity. The general objective of 'training' the neural network is to modify the connection weights to reduce the errors between the actual target outputs to a satisfactory level. This process is carried out through the minimization of the defined error function using the gradient descent approach. After convergence occurs (i.e. the errors are minimal), the associated trained weights of the model are tested with a separate set of testing data. This testing is used to assess the generalization capability of the trained model to produce the correct input-output mapping.

Even after obtaining the limit state surface, due to the uncertainties in the design parameters (random variables) in the limit state surface, it is impossible to predict the state of the system with accuracy. The alternative is to assess the probability of failure P_f. The calculation of P_f involves the determination of the joint probability distribution of R and S and the integration of the Probability Density Function (PDF) over the failure domain. For a problem with multiple n random variables, the calculation of P_f involves the determination of a multi-dimensional joint PDF of the random variables and the integration of the PDF over the failure domain.

A well-developed approximate alternative is to use the First-Order Reliability Method (FORM) [8]. Its popularity results from the mathematical simplicity, since only second moment information (mean and standard deviation) on the random variables is required to calculate the reliability index β. Some examples of the use of FORM in rock mechanics have been presented [9, 10]. Mathematically, β can be computed [11] as

$$\beta = \min_{x \in F} \sqrt{(\frac{x_i - \mu_i}{\sigma_i})^T [\mathbf{R}]^{-1} (\frac{x_i - \mu_i}{\sigma_i})} \qquad (2)$$

in which x_i is the set of n random variables, μ_i is the set of mean values, $\boldsymbol{R}$ is the correlation matrix and F is the failure region. The minimization in Eq. (2) is performed over F corresponding to the region $G(\boldsymbol{x}) = 0$. Low and Tang [11] had shown that an EXCEL (Microsoft) spreadsheet environment can be used to perform the minimization and determine β. If the random variables have probability distributions close to normal, then P_f can be obtained from the expression:

$$P_f \approx \Phi(-\beta) \qquad (3)$$

in which $\Phi(-\beta)$ is the value of the cumulative probability. This value can be obtained from tables of the standard cumulative normal distribution function found in many textbooks or from built-in functions in most spreadsheets.

This paper utilizes the rock mass classification correlations and the numerical procedure known as the shear strength reduction technique to calculate the global factor of safety *FS* with regard to stress-induced instability. The BPNN is used to determine an empirical equation relating *FS* to the cavern dimensions *B* and *H*, as well as the rock mass quality *Q*. Charts based on this equation are presented for preliminary design purposes. A FORM spreadsheet is implemented with the neural network algorithm to calculate the reliability index (probability of failure) for cavern stability.

2. Numerical model of rock cavern

The FLAC^{3D} code (Itasca) was used to carry out the stability analyses of the underground rock caverns using the shear strength reduction technique. The shear strength reduction technique is available in many commercial finite element and finite difference programs. The technique has been applied to a number of geotechnical problems including rock caverns [12,13] and circular tunnels [14].

The procedure essentially involves repeated analyses by progressively reducing the shear strength properties until collapse occurs. For a Mohr-Coulomb material, by reducing the shear strength by a factor *F* the shear strength equation becomes:

$$\frac{\tau}{F} = \frac{c}{F} + \sigma_n \frac{\tan\phi}{F} \tag{4}$$

$$F = \frac{\tau}{c^* + \sigma_n \tan\phi^*} \tag{5}$$

where τ is the shear strength, σ_n is the normal stress, and $c^* = \frac{c'}{F}$ and $\phi^* = \arctan(\frac{\tan\phi}{F})$ are the new Mohr-Coulomb shear strength parameters. Systematic increments of *F* are performed until the finite element or finite difference model does not converge to a solution (i.e. failure occurs). The critical strength reduction value which corresponds to non-convergence is taken to be the factor of safety *FS*.

Only stress-induced failure was considered in this paper. In the FDM analyses, the three parameters that were varied were: the Tunneling Quality Index *Q* value, the cavern width *B* and cavern wall height *H*. *Q* cannot be directly used in the FLAC^{3D} calculations, though it is a commonly used quality index representing rock mass competence. In the analyses, the discontinuous nature of the rock is incorporated implicitly in the Mohr-Coulomb constitutive relationship used to represent the mass as an equivalent continuum. The rock mass properties are indirectly (through *RMR*) determined from the *Q* value by means of empirical equations as shown in Table 1. The *Q* value of each category and its corresponding Mohr-Coulomb rock properties to be used in the numerical calculation are shown in Table 2, in which the *c*, ϕ and *E* values are related to *Q* through the equations in Table 1. It should be noted that these relationships are intended to provide the initial estimates of the rock mass properties and should be used with caution in engineering design. It should also be pointed out that numerical analyses with the in-situ stress ratio K_0 in the range of 1 to 3 were also carried out. While the K_0 was found to significantly influence the state of stress and magnitude of displacements in proximity to the cavern, it had minimal influence on the *FS* and was therefore omitted as one of the design variables.

Table 1 Empirical equations relating *Q* with rock mass properties

Table 2 Rock mass properties with different *Q* values

The cross-section of the cavern and boundary conditions are shown in Fig. 1. The cavern roof arc is semi-circular and the overburden height *D* from the ground surface to the top of the side wall is 100 m. The cavern length in the longitudinal direction is assumed as 1 m to simulate plane strain conditions. Outer boundaries are located far from the cavern to minimize the boundary effects. Full-face excavation is assumed in all analyses. Table 3 lists the design parameters and the values that were considered. Input file for each FLAC^{3D} execution includes a geometry model (*B* and *H*) and a mechanical model of *Q*-related rock mass properties.

Fig. 1. Underground cavern configuration.

Table 3 Input parameters for safety factor calculations

For each numerical analysis, the safety factor *FS* was determined based on the strength reduction technique. Different combinations of *Q*, the cavern width *B* and the side cavern height *H* were considered for three sets of ratios of *B* and *H* (*B/H* = 1, 2 and = 4). A total of 216 cases were considered and some results are shown in Table 4. A typical plot of *Q* versus *FS* for *B* = 20 m in Fig. 2 indicates the *FS* decreases as *H* increases.

Table 4 Some calculations for safety factor *FS*

Fig. 2. Plot of *FS* versus *Q* for *B* = 20 m.

3. Determination of limit state surface using neural networks

In this study, the three input neurons are *Q*, cavern width *B* and wall height *H*. The output neuron is the corresponding *FS* values determined from the FDM analyses. Of the 216 data sets, 162 patterns were randomly selected as the training data and the remaining 54 data were used for testing. From a trial-and-error process, eight hidden neurons and the ‘tansig’ transfer function were found to be the optimal architecture. A comparison of the calculated and predicted *FS* values presented in Fig. 3 shows very good agreement with R^2 greater than 0.99.

Fig. 3. Neural network results.

For comparison, the predictions using logarithmic regression method are also presented. The best fit logarithmic regression equation with a coefficient of correlation $R^2 = 0.96$ was as follows:

$$FS_{regression} = 2.469Q^{0.1759}B^{-0.2763}H^{-0.0973} \quad (6)$$

The results of the actual *FS* determined from FDM versus the predicted *FS* using Eq. (6) as shown in Fig. 4 show that the BPNN model predictions were more accurate.

Fig. 4. Logarithmic regression.

Using the optimal trained connection weights, it is possible to develop a mathematical expression relating the input variables and the output variable (predicted *FS*) [18]. The mathematical expression for *FS(Q, B, H)* obtained by the neural network analysis is shown in the Appendix. Based on this mathematical expression for *FS(Q, B, H)* obtained, a series of charts relating *FS* to Tunneling Quality Index *Q* and the cavern geometries *B* and *H* have been developed as shown in Fig. 5. Also shown in Fig. 5 are the curves determined using Eq. (6) which generally exhibit similar trends as the curves developed using the neural network algorithm. The proposed charts in Fig. 5 are potentially useful for preliminary design and checking. Similar charts have been proposed for the design of mining stope panels [19].

Fig. 5. Design curves for cavern *FS* for different *B/H* ratios: (a) *B/H* = 1; (b) *B/H* = 2 and (c) *B/H* = 4.

4. Reliability Analysis

Using the optimal trained connection weights and the mathematical relationship to determine FS_{NN} shown in the Appendix, it is possible to perform reliability analysis as outlined below. Assuming the limiting factor of safety $FS_{lim} = 1$, the limit state surface is defined as $G(\boldsymbol{x}) = FS_{NN} - 1$ and incorporated into an EXCEL spreadsheet environment based on the approach by Low and Tang [11] from which the reliability index β can be determined. Fig. 6 shows a sample spreadsheet for computing the reliability index where *Q*, *B* and *H* are assumed to be lognormally distributed. The spreadsheet cells A2:A4 allows the selection of various distribution types for the input variables, including normal, lognormal, triangular etc as explained in Low and Tang [11]. For nonnormals, the nonnormal distributions are replaced by an equivalent normal ellipsoid,

centered at the equivalent normal mean. Cells C2:F4 are parameters which are set corresponding to the variable distribution types. For lognormals, cells C2:C4 correspond to the mean values while cells D2:D4 correspond to the standard deviations. The correlation matrix [***R***] cells K2:M4 are used to define the correlations between *Q*, *B* and *H*. The n_i vector in cells N2:N4 contains equations for $(x_i - \mu_i^N)/\sigma_i^N$ as defined in Eq. (2). Cells H2:J9 contain the weights and algorithms obtained from the trained neural network. The design point (*x** values) was obtained by using the spreadsheet's built-in optimization routine SOLVER to minimize the cell, by changing the *x** values, under the constraint that the performance function $G(x^*) = 0$. Prior to invoking the SOLVER search algorithm, the *x** values were set equal to the mean values (4, 20, 20) of the original random variables. Iterative numerical derivatives and directional search for the design point *x** were automatically carried out in the spreadsheet environment.

Fig. 6. Sample spreadsheet using FORM.

The spreadsheet algorithm was also verified through the use of Monte Carlo simulation. For brevity this has been omitted. In all the results presented in this paper, the standard deviation for both *B* and *H* were 0.5 m. Generally the sensitivity analyses indicated that variations of the standard deviations of up to 0.5 m for both *B* and *H*, did not significantly influence the P_f. For brevity these results have been omitted. Instead, this paper focuses on the influence of *Q* on P_f.

To better illustrate the influence of the *Q* value on β and P_f, the effects of the coefficient of variation of *Q* (Cov_Q) and the mean value of *Q* (m_Q) are integrated into a single figure. The effects of changing the mean value of *Q* while keeping all other parameters constant are illustrated in Fig. 7. Also shown in Fig. 7 are the corresponding safety factors computed by the FDM. Both approaches show that an increase in the *Q* mean value (higher strength) will result in a higher *FS* and a reduction in P_f.

In general the safety factor may vary linearly or nonlinearly as the mean values change, depending on whether the safety factor is a linear or nonlinear function of the particular parameter. P_f, however, always varies nonlinearly. Above a certain *FS* value, P_f approaches asymptotically to zero. Any further increase of *FS* will have negligible effect on the failure probability of the underground rock cavern. In the case of cavern stability analysis, both *FS* and

P_f vary monotonously for the variables, i.e. either monotonously increasing or monotonously decreasing. It should be highlighted that even for the case where the safety factor equals 1.5, for the case with Cov_Q = 0.6, P_f is approximately 12%. This demonstrates that a single *FS* value obtained from deterministic method may not always provide an adequate quantification of safety.

Fig. 7. Effects of changing the characteristic values of Q (B = 20 m, H = 10 m): (a) β vs. Q under different Cov_Q and (b) P_f vs. Q under different Cov_Q.

The effects of Cov_Q while keeping other parameters constant are also illustrated in Fig. 7. With increase in Cov_Q, even with FS > 1.0, P_f could increase to close to 25% (Cov_Q = 0.6).

The plots in Fig. 7 show P_f as a function of Cov_Q at different *FS* levels. The plots show that in order to achieve the same target P_f would require different safety factors, depending on the magnitude of the standard deviations. For example, for a target failure probability of 10% will require a *FS* of 1.31 if Cov_Q = 0.4 and a *FS* of 1.50 if Cov_Q = 0.6. The results highlight that there is a degree of uncertainty involved in the stability of the underground rock cavern and the variations of the design parameters play an important role, which the conventional safety factor analysis cannot reflect. However, it is not advocated here that factor of safety analyses be abandoned in favor of reliability analyses. Instead, it is suggested that the factor of safety and reliability approaches be used together, as complementary measures of acceptable design [20].

P_f values for the three sets of B and H are integrated in Fig. 8 for comparison. The results show that for the same Q mean value, a larger cavern (B = 20 m, H = 20 m) results in a smaller *FS*. Also for the same Q mean value and the same Cov_Q, a larger cavern (B = 20 m, H = 20 m) results in a higher P_f (for Cov_Q = 0.4 and m_Q = 4, $P_f \approx$ 41% for B = 20 m and H = 20 m while $P_f \approx$ 11% for B = 20 m and H = 10 m).

Fig. 8. The probability of failure values for the three sets of B and H.

5. Summary and conclusions

Numerical analyses have been carried out using the finite difference method to assess the global stability of underground rock caverns. Analyses using neural networks were used to model the relationship between Q, B and H, and the cavern safety factor *FS*. A comparison of the

calculated and predicted *FS* values showed very good agreement with a coefficient of correlation R^2 greater than 0.99. Using the optimal trained connection weights of the neural network model, charts relating *FS* to *Q* and the cavern geometries have also been developed. The proposed charts in Fig. 5 are potentially useful for preliminary stability design and checking.

The first order reliability algorithm and built-in spreadsheet optimization routine were incorporated with the neural network algorithm to calculate the reliability index for cavern stability. The reliability analyses indicated that the probability of failure is significantly influenced by the coefficient of variation of *Q*. This highlights the point that a single safety factor cannot provide the complete information regarding the cavern stability as the same safety factor may indicate completely different probabilities of failure for different coefficient of variations of *Q*. It is suggested that the factor of safety and probability of failure (reliability index) approaches be used together, as complementary measures of acceptable design.

This study will be extended to consider underground caverns that account for other relevant excavation factors such as 3D effects, excavation rate and rock bolt system. Furthermore, a full-scale ground model and the spatial variation of *RMR* or *Q* described through Geo-statistical analysis as outlined in [21] will be considered for subsequent detailed stability design. In addition, for simplicity, in this study the shape of the cavern roof has been assumed as semi-circular. Various other shapes such as an elliptical or horse-shoe shape will also be considered.

Acknowledgements

The authors thank the Defense Science and Technology Agency Singapore for providing the research funding for this project.

Appendix

The transfer functions used for BPNN neural network output for stability are ‘tansig’ transfer function for hidden layer to output layer and ‘purelin’ transfer function for output layer to target. The calculation process of BPNN output for stability is elaborated in detail as follows:

From the connection weights for a trained neuron network, it is possible to develop a mathematical equation relating the input parameters and the single output parameter *Y* using

$$[A1]\ Y = f_{sig}\left\{b_0 + \sum_{k=1}^{h}\left[w_k\, f_{sig}\left(b_{hk} + \sum_{i=1}^{m} w_{ik} X_i\right)\right]\right\}$$

in which b_0 is the bias at the output layer, w_k is the weight connection between neuron k of the hidden layer and the single output neuron, b_{hk} is the bias at neuron k of the hidden layer (k = 1, h), w_{ik} is the weight connection between input variable i (i =1, m) and neuron k of the hidden layer, X_i is the input parameter i, and f_{sig} is the sigmoid (tansig & purelin) transfer function.

Using the connection weights of the trained neural network, the following steps can be followed to calculate *FS(Q,B,H)*:

Step1: Normalize the input values for *Q*, *B* and *H* linearly using

$$x_{norm} = 2(x_{actual} - x_{min})/(x_{max} - x_{min}) - 1$$

Let the actual $Q = X_{1a}$ and the normalized $Q = X_1$

$X_1 = -1+2*(X_{1a} - 0.1)/399.9$

Let the actual $B = X_{2a}$ and the normalized $B = X_2$

$X_2 = -1+2*(X_{2a} - 2)/48$

Let the actual $H = X_{3a}$ and the normalized $H = X_3$

$X_3 = -1+2*(X_{3a} - 0.5)/49.5$

Step2: Calculate the normalized deflection (Y_1) using the following expressions:

$A_1 = -9.9763+0.1056X_1-4.2526X_2-3.5310X_3$

$A_2 = -2.4331-0.0274X_1-0.3828X_2-0.1653X_3$

$A_3 = -3.3351-1.2762X_1-0.2816X_2-0.0850X_3$

$A_4 = 0.7064-2.8993X_1+1.0173X_2+0.0204X_3$

$A_5 = -100.0669-98.7342X_1-0.0819X_2-0.0331X_3$

$A_6 = -35.4801-27.2544X_1-3.4444X_2-2.8153X_3$

$A_7 = 0.7589-3.1429X_1+1.1580X_2+0.0220X_3$

$A_8 = -108.7918-108.0597X_1-0.0909X_2-0.0356X_3$

$B_1 = 21.8108\times\tanh(A_1)$

$B_2 = 26.6348\times\tanh(A_2)$

$B_3 = -12.1562\times\tanh(A_3)$

$B_4 = 8.1846\times\tanh(A_4)$

$B_5 = -60.5545\times\tanh(A_5)$

$B_6 = -8.5957\times\tanh(A_6)$

$B_7 = -8.1304\times\tanh(A_7)$

$B_8 = 20.2019\times\tanh(A_8)$

$C_1 = -13.4345+ B_1+ B_2+ B_3+B_4+B_5+B_6+B_7+B_8$

$Y_1 = C_1$

Step3: De-normalize the output to obtain the safety factor FS_{NN}

$FS_{NN} = 0.28+5.09\times(Y_1+1)/2$

References

[1] Bieniawski ZT. Engineering rock mass classifications. New York: Wiley and Sons; 1989.

[2] Barton N. Lien R. Lunde J. Engineering classification of rock masses for the design of tunnel support. Rock Mech 1974; 6:183–236.

[3] Meguid MA, Rowe RK. Stability of D-shaped tunnels in a Mohr-Coulomb material under anisotropic stress conditions. Can Geotech J 2006; 43:273–281.

[4] Hatzor YH, Talesnick M, Tsesarsky M. Continuous and discontinuous stability analysis of the bell-shaped caverns at Bet Guvrin, Israel. Int J Rock Mech Min Sci 2002; 39:867–886.

[5] Cundall PA. Explicit finite difference methods in geomechanics, numerical methods in engineering. In Proceedings of the EF Conference on Numerical Methods in Geomechanics, Blacksburg, Virginia 1976; 1:132–150.

[6] Shi GH. Discontinuous deformation analysis-a new model for the statics and dynamics of block systems. PhD Thesis, University of California, Berkeley; 1988.

[7] Bobet A, Fakhimi A, Johnson S, Morris J, Tonon F, Yeung M. Numerical models in discontinuous media: A review of advances for rock mechanics applications. J Geotech Geoviron 2009; 135(11): 1547–1561.

[8] Hasofer AM, Lind NC. An exact invariant first-order reliability format. J Eng Mech 1974; 100:111–121.

[9] Low BK. Efficient probabilistic algorithm illustrated for a rock slope. Rock Mech Rock Eng 2008; 41(5):715–734.

[10] Li HZ, Low BK. Reliability analysis of circular tunnel under hydrostatic stress field. Comput Geotech 2010; 37:50–58.

[11] Low BK, Tang WH. Efficient spreadsheet algorithm for first order reliability method. J Eng Mech 2007; 133(12): 1378–1387.

[12] Hammah RE, Yacoub T, Curran JH. Serviceability-based slope factor of safety using the shear strength reduction (SSR) method. The Second Half Century of Rock Mechanics 11th Congress of the International Society for Rock Mechanics 2007, Taylor & Francis, 1137–1140,

[13] Zhang WG, Goh ATC. Reliability assessment on ultimate and serviceability limit states and determination of critical factor of safety for underground rock caverns. Tunneling and Underground Space Technology 2011. Under review.

[14] Vermeer PA, Ruse N, Marcher T. Tunneling heading stability in drained ground. Felsbau, Jg 2002. 20(6): 8–18.

[15] Tugrul A. The application of rock mass classification systems to underground excavation in weak lime stone, Ataturk dam, Turkey. Eng Geo 1998; 50(3-4): 337–345.

[16] Bieniawski ZT. Determining rock mass deformability: experience from case histories. Int J Rock Mech Min Sci Geomech Abstr 1978; 15:237–247.

[17] Serafim JL, Pereira JP. Considerations of the geomechanics classification of Bieniawski. In Proc of Int Symp Eng Geol Underground Construction, LNEC, Lisbon, 1983; 1(II): 33–42.

[18] Goh ATC, Kulhawy FH. Neural network approach to model the limit state surface for reliability analysis. Can Geotech J 2003; 40:1235–1244.

[19] Houghton DA, Stacey TR. Application of probability techniques to underground situations. Proc 7th Regional Conf for Africa on Soil Mech & Foundation Eng. Accra, Vol 2, Balkema 1980; 879–883.

[20] Duncan JM. Factors of safety and reliability in geotechnical engineering. J Geotech Geoviron 2000; 126 (4): 307–316.

[21] Exadaktylos G, Stavropoulou M. A specific upscaling theory of rock mass parameters exhibiting spatial variability: Analytical relations and computational scheme. International Journal of Rock Mechanics & Mining Sciences 2008; 45:1102–1125.

List of Tables

List of Figures

Table1

Table 1 Empirical equations relating *Q* with rock mass properties.

Properties	Equations	References
RMR from *Q* value	$RMR = 7\ln Q + 36$	[15]
Cohesion *c* (MPa)	$c(MPa) = 0.005(RMR - 1)$	[1]
Friction angle ϕ (°)	$\phi = 0.5RMR + 4.5$	[1]
Deformation modulus *E* (GPa)	$E = E_m(GPa) = 2RMR - 100\ (RMR > 50)$ $E = E_m(GPa) = 10^{(RMR-10)/40}\ (RMR \le 50)$	[16-17]

Table2

Table 2 Rock mass properties with different *Q* values.

Q	*c* (MPa)	ϕ (°)	*E* (GPa)	Poisson's ratio
Q = 0.1	0.07	12.23	1.37	0.35
Q = 0.4	0.14	19.29	3.09	0.35
Q = 1	0.18	22.50	4.47	0.35
Q = 4	0.22	27.35	7.81	0.20
Q = 10	0.26	30.56	11.30	0.20
Q = 40	0.30	35.41	19.75	0.16
Q = 100	0.34	38.62	28.57	0.16
Q = 400	0.38	43.47	49.95	0.16

Table3

Table 3 Input parameters for safety factor calculations

Input Parameters	Values
Q value	0.1, 0.4, 1, 4, 10, 40, 100, 400
Cavern width *B* (m)	2, 5, 10, 15, 20, 25, 30, 40, 50
Side wall height *H* (m)	0.5, 1, 1.25, 2, 2.5, 3.75, 5, 6.25, 7.5, 10, 12.5, 15, 20, 25, 30, 40, 50

Table4

Table 4 Some calculations for safety factor *FS*

Q	***B* (m)**	***B/H***	***FS***	***Q***	***B* (m)**	***B/H***	***FS***
0.1	10	1	0.57	0.1	20	1	0.43
0.4	10	1	1	0.4	20	1	0.76
1	10	1	1.21	1	20	1	0.92
4	10	1	1.51	4	20	1	1.14
10	10	1	1.77	10	20	1	1.34
40	10	1	2.08	40	20	1	1.58
100	10	1	2.37	100	20	1	1.8
400	10	1	2.72	400	20	1	2.07
0.1	10	2	0.62	0.1	20	2	0.47
0.4	10	2	1.08	0.4	20	2	0.82
1	10	2	1.32	1	20	2	1.01
4	10	2	1.65	4	20	2	1.26
10	10	2	1.93	10	20	2	1.47
40	10	2	2.27	40	20	2	1.73
100	10	2	2.58	100	20	2	1.97
400	10	2	2.96	400	20	2	2.27
0.1	10	4	0.65	0.1	20	4	0.49
0.4	10	4	1.14	0.4	20	4	0.87
1	10	4	1.41	1	20	4	1.07
4	10	4	1.75	4	20	4	1.33
10	10	4	2.03	10	20	4	1.54
40	10	4	2.39	40	20	4	1.82
100	10	4	2.72	100	20	4	2.07
400	10	4	3.12	400	20	4	2.38

Figure1

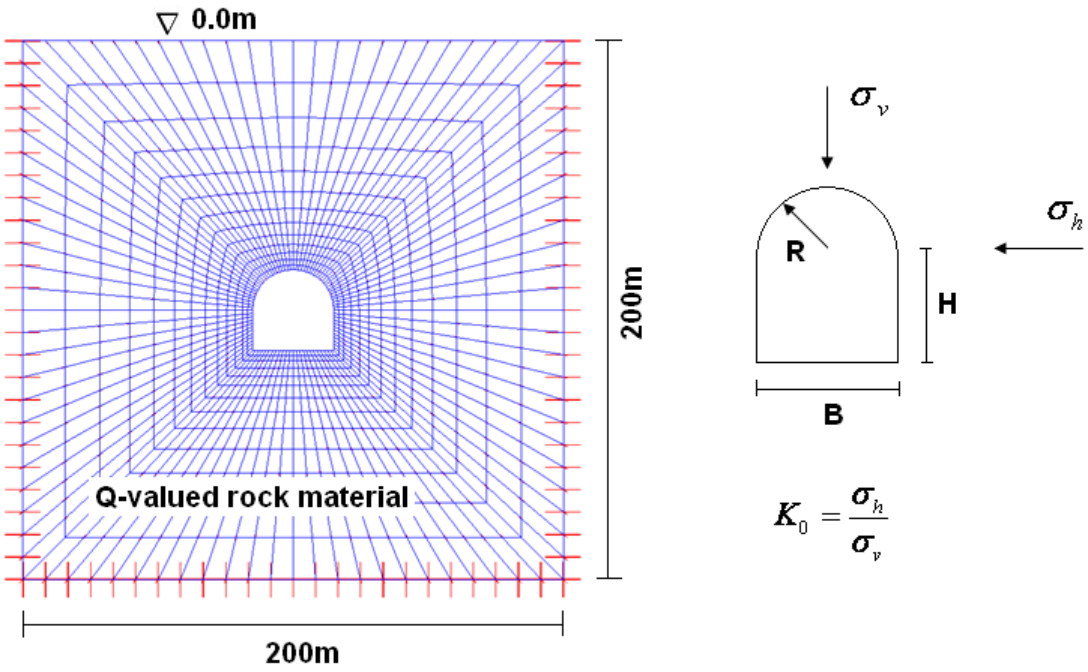

Fig.1. Underground cavern configuration.

Figure2

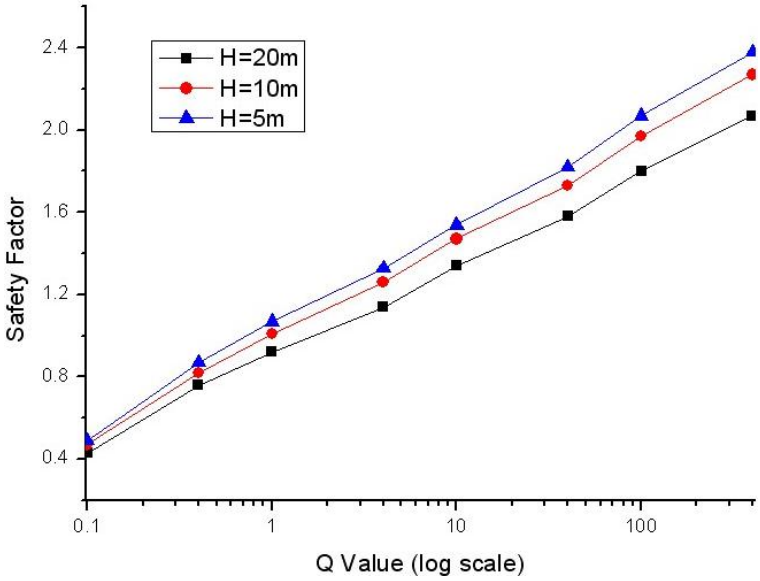

Fig.2. Plot of *FS* versus *Q* for *B* = 20 m

Figure3

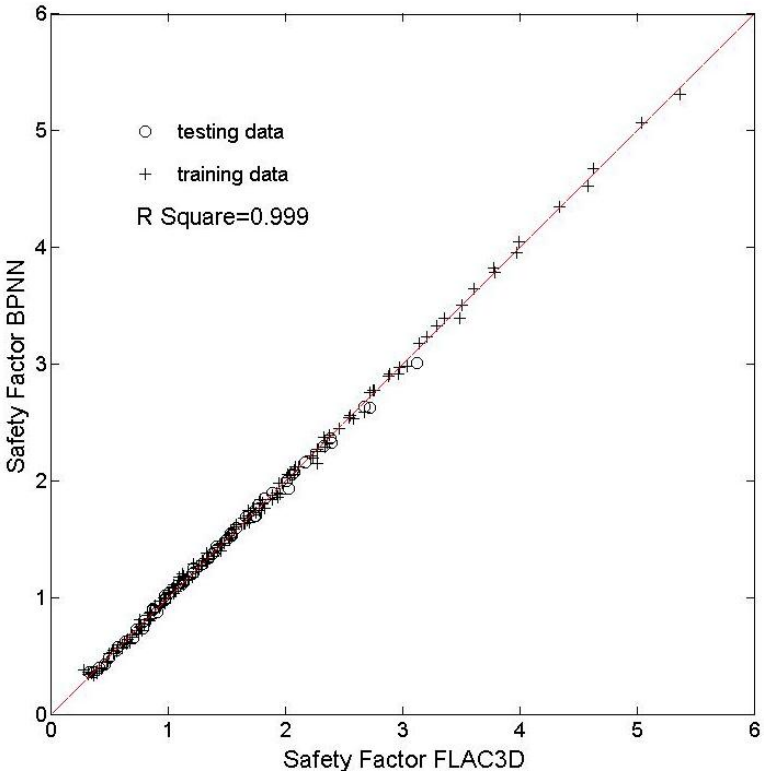

Fig.3. Neural network results.

Figure4

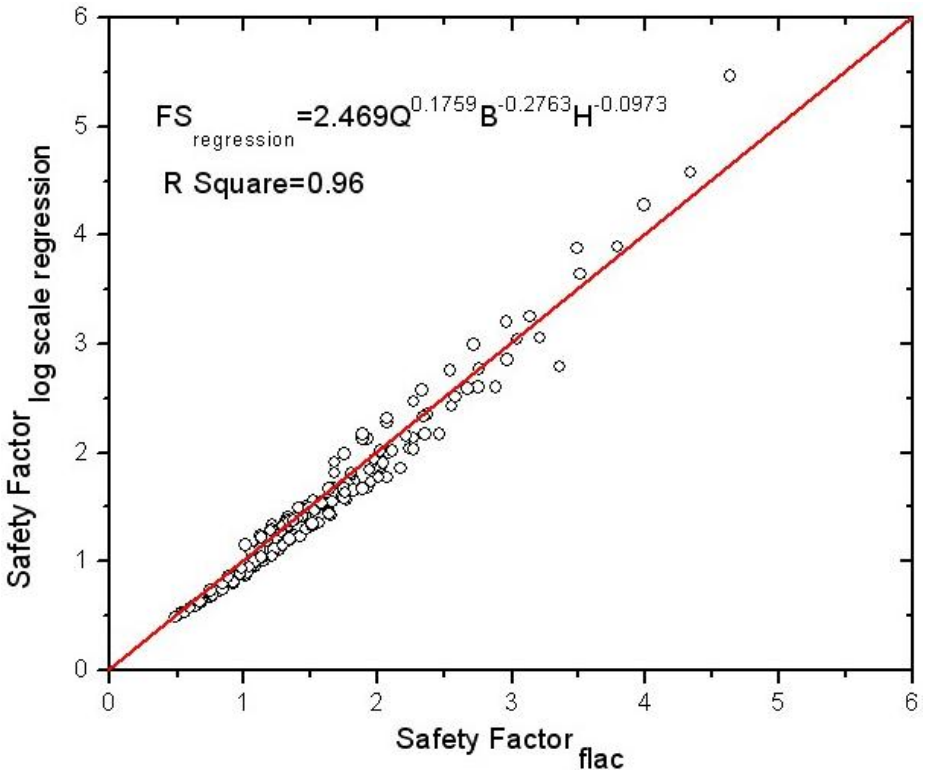

Fig.4. Logarithmic regression.

Figure5

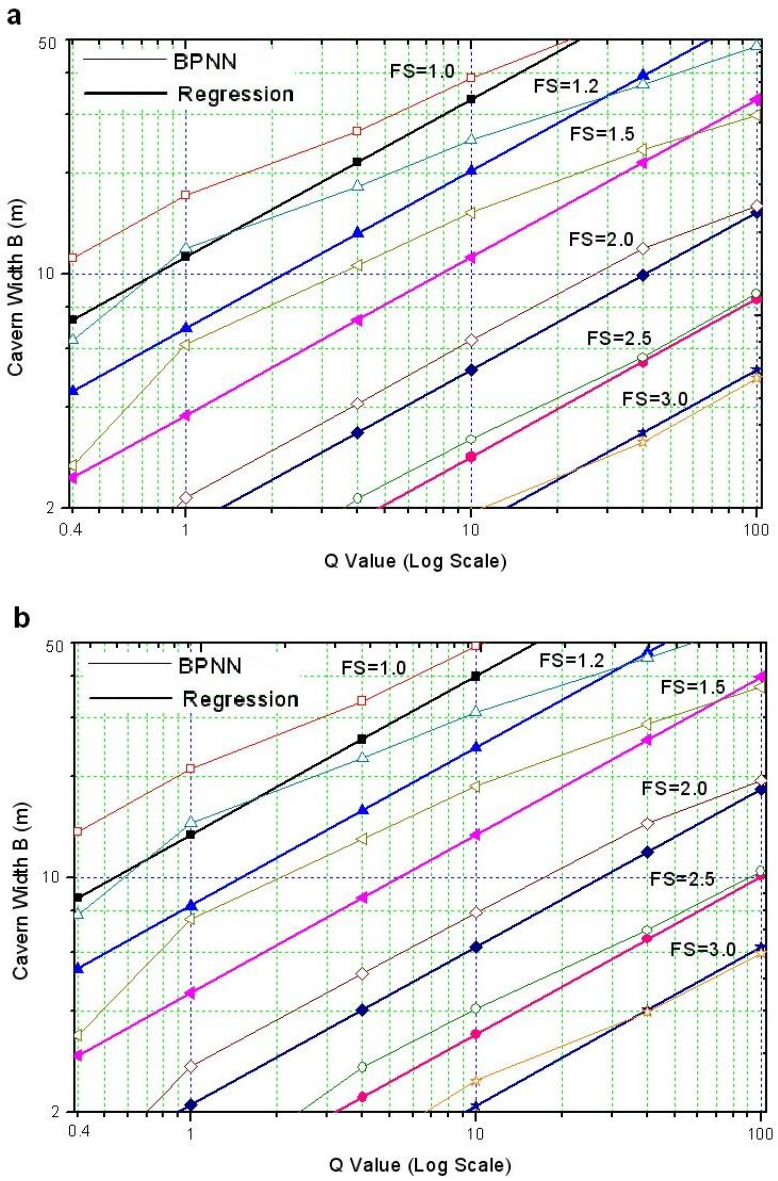
a
BPNN
Regression
FS=1.0
FS=1.2
FS=1.5
FS=2.0
FS=2.5
FS=3.0
Cavern Width B (m)
Q Value (Log Scale)
50
10
2
0.4
1
10
100
b
BPNN
Regression
FS=1.0
FS=1.2
FS=1.5
FS=2.0
FS=2.5
FS=3.0
Cavern Width B (m)
Q Value (Log Scale)
50
10
2
0.4
1
10
100

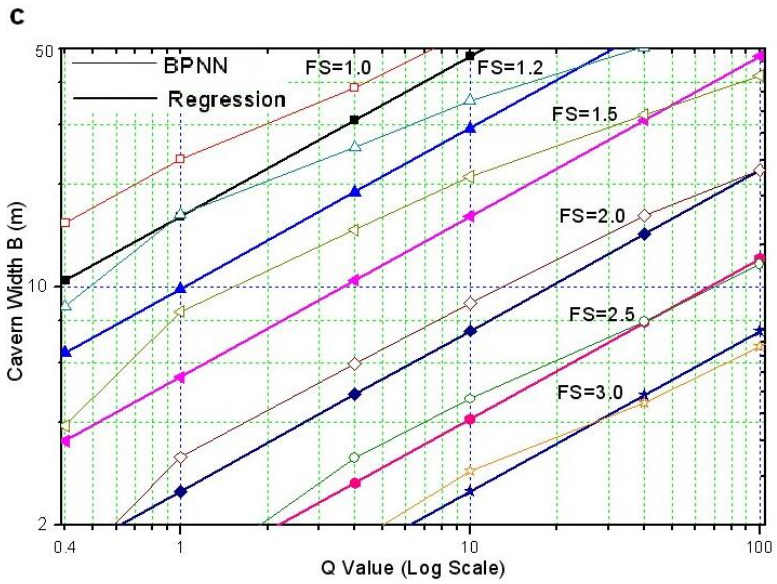

Fig. 5. Design curves for cavern *FS* for different *B/H* ratios: (a) *B/H* = 1; (b) *B/H* = 2 and (c) *B/H* = 4.

Figure6

	A	B	C	D	E	F	G	H	I	J	K	L	M	N	O	P	Q
1	Distribution	Variables	Para1	Para2	Para3	Para4	x_i^*	BPNN PROCESS			Correlation matrix [R]			n_i	g(x)	β	P_f(%)
2	Lognormal	Q	4	0.8			2.62121	-0.987	-8.305	-21.81	1	0	0	-2.035	-1E-10	2.0632	1.9548
3	Lognormal	B	20	0.5			20.1363	-0.244	-2.278	-26.08	0	1	0	0.2842			
4	Lognormal	H	20	0.5			20.0862	-0.209	-1.988	11.709	0	0	1	0.1845			
5									3.3163	8.1631							
6									-2.551	59.822							
7									-7.14	8.5957							
8									3.5747	-8.118							
9									-2.065	-19.56							

Fig.6. Sample spreadsheet using FORM.

Figure7

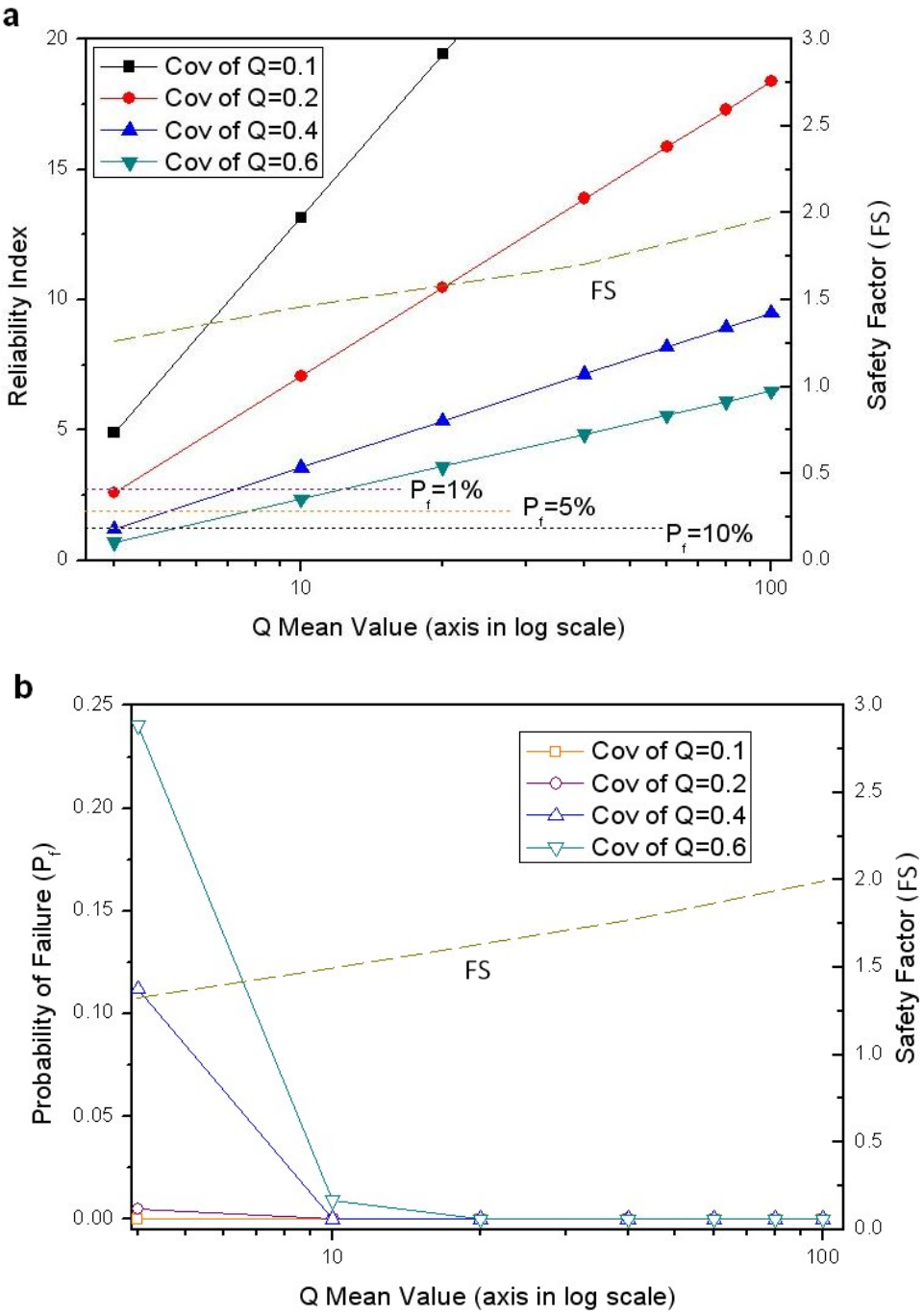

Fig.7. Effects of changing the characteristic values of Q (B = 20 m, H = 10 m): (a) β vs. Q under different Cov_Q and (b) P_f vs. Q under different Cov_Q

Figure8

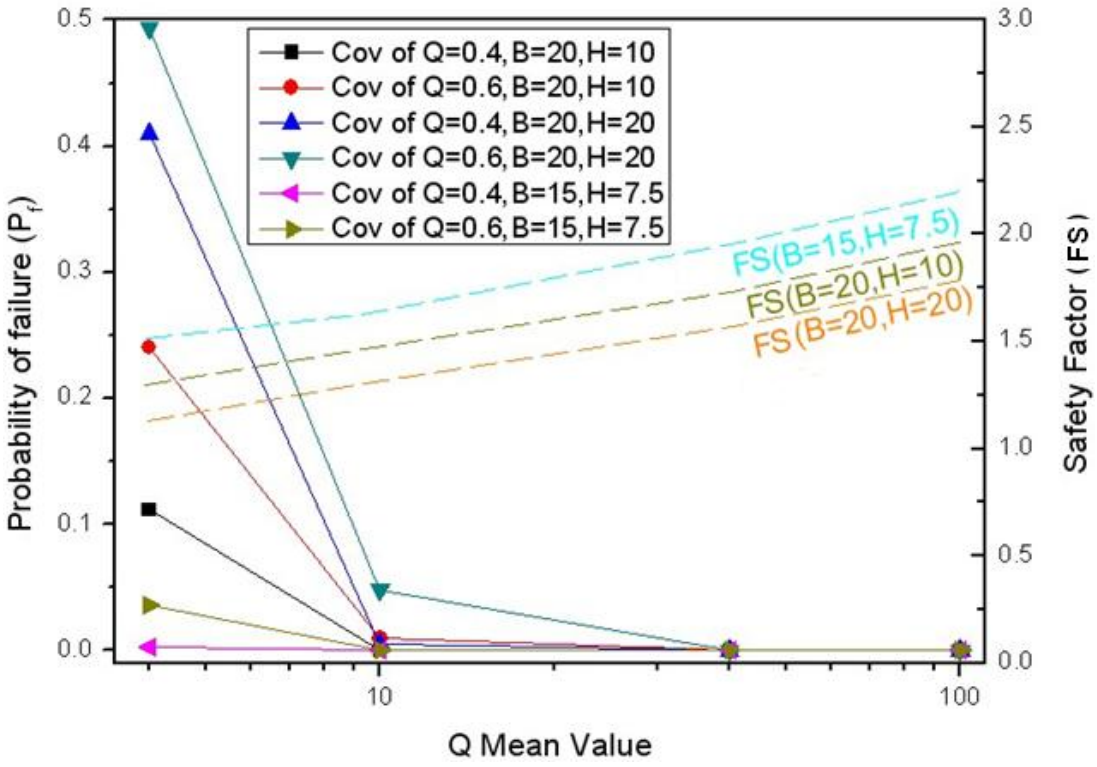

Fig.8. The probability of failure values for the three sets of *B* and *H*.